Charm mixing with $\mathrm{D}^0 \to \mathrm{K}\pi\pi^0$ decays at LHCb

Serena Maccolini *
University of Bologna, Italy

Abstract

The work here presented reports a first preliminary study of charm mixing using $D^0 \to K^+\pi^-\pi^0$ decays reconstructed in a data sample corresponding to 2 fb^{-1} of integrated luminosity collected by LHCb in 2012. In addition, prospects for Run 2 have been evaluated and are also discussed.

1 Introduction

Charm mixing refers to spontaneous $D^0 \to \bar{D}^0$ and $\bar{D}^0 \to D^0$ transitions occurring in the time evolution of neutral mesons before decaying [1]. This process is a manifestation of flavour-changing neutral currents that occurs because of the charm flavour-defined states, D^0 and $\bar{D}^0$ differ from the physical mass eigenstates, D_1 and D_2, and is characterized by the normalized mass and decay width differences between the two mass eigenstates

$$x = \frac{m_1 - m_2}{\Gamma} \quad \text{and} \quad y = \frac{\Gamma_1 - \Gamma_2}{2\Gamma},$$

where Γ is the average decay width.

Short-range quark-level transitions as well as long-range processes contribute to this phenomenon. The former are governed by loops in which virtual heavy particles are exchanged, making the study of flavour oscillations an attractive area to search for physics beyond the Standard Model. Studies on charm mixing are particularly interesting because it can be sensitive to new physics coupled to the up-type sector.

The first evidence for $D^0 - \bar{D}^0$ oscillation was reported in 2007 by the B-factories [2, 3]. In 2012 the LHCb experiment reported the first observation from a single measurement using decays to the two body $K^+\pi^-$ final state [4]. The current world averages for the mixing parameters, as reported by the *Heavy Flavor Averaging Group* when combining all available mixing measurements [5], do not conclusively show whether x deviates or not from zero. To improve our knowledge of x, it is crucial to study charm mixing with many and different decay channels, and in particular decays to multi-body final states. The goal of this project is to perform, for the first time in LHCb, a preliminary study of charm mixing using $D^0 \to K^+\pi^-\pi^0$ decays.

Charm mixing is here studied by measuring the ratio of $D^0 \to K^+\pi^-\pi^0$ to $D^0 \to K^-\pi^+\pi^0$ decay rates (charge-conjugated decays are implied). The neutral D meson flavour at production time is determined using the charge of the soft (low-momentum) pion π_S in the flavour-conserving $D^{\star\pm} \to \overset{(-)}{D}{}^0\pi_S^\pm$ decay. The $D^{\star+} \to D^0(\to K^-\pi^+\pi^0)\pi_S^+$ process is referred to as right-sign (RS), whereas the $D^{\star+} \to D^0(\to K^+\pi^-\pi^0)\pi_S^+$ is designated as wrong-sign (WS). As graphically shown in Fig. 1, the RS process is dominated by a Cabibbo-favoured (CF) decay amplitude, whereas the WS amplitude includes contributions from both the direct double-Cabibbo-suppressed (DCS) $D^0(\to K^+\pi^-\pi^0)$ decay, as well as $D^0 - \bar{D}^0$ mixing followed by the CF $\bar{D}^0(\to K^+\pi^-\pi^0)$ decay.

*under the supervision of Angelo Di Canto (CERN)

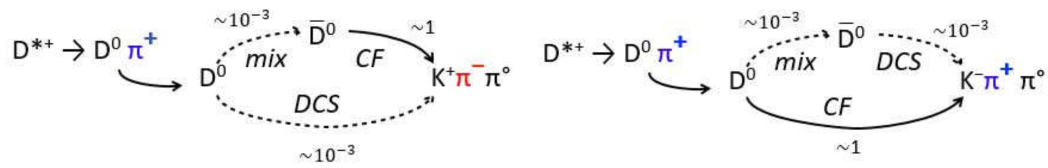

(a) (b)

Figure 1: Scheme of WS (a) and RS (b) decays where the $D^{\star}$ decays in $D^0\pi_S$ and D^0 decays in $K\pi\pi^0$. An event is defined WS (RS) when the two pions have different (same) charge. In the scheme the $D^{\star}$ decay is flavour-conserving while in D^0 decay there is the contribution of Cabibbo-favoured (CF), double-Cabibbo-suppressed (DCS) and mixing processes.

Since the observed mixing parameters are small [5], the time-dependent ratio $R(t)$ of WS to RS decays rates, assuming negligible CP violation, can be approximated by the following quadratic expression:

$$R(t) = \frac{WS(t)}{RS(t)} \approx R_D + \alpha\sqrt{R_D}y'\left(\frac{t}{\tau}\right) + \frac{R_M}{2}\left(\frac{t}{\tau}\right)^2 \tag{1}$$

where t/τ is the decay time expressed in units of the average D^0 lifetime. The time-independent term R_D corresponds to the ratio of DCS to CF decay rates integrated over the Dalitz space. The quadratic term is proportional to the mixing rate $R_M = (x^2 + y^2)/2$, which is instead independent of the Dalitz space. The linear term is due to the interference between the DCS and the mixing amplitudes. Here $y' = y\cos(\delta) - x\sin(\delta)$ with δ being a Dalitz-integrated strong phase difference between the DCS and the CF amplitudes, while $0 \leq \alpha \leq 1$ is the coherence factor and accounts for strong-phase variations over the Dalitz space. In this channel the coherence factor is measured to be 0.82 ± 0.07 [6], so large enough to make this channel particularly interesting for mixing studies since the sensitivity to mixing comes mostly from linear term in decay time.

The available experimental measurements of mixing using $D^0 \to K^+\pi^-\pi^0$ come from the B-factories experiments: Belle measures only the time- and Dalitz-integrated ratio R [7]; BaBar has two results, the first measures R and the Dalitz-integrated quantities R_D, $\alpha y'$ and R_M [8], the second measures the mixing parameters x', y' using a time- and Dalitz-dependent analysis [9].

2 Overview of the project

The first task of the project is the selection of the candidates described in § 3 and § 4, using Run 1 data. The yields of RS and WS signal are extracted by fitting the $M_{D^0\pi_S}$ distribution and the time- and Dalitz-integrated WS-to-RS ratio is measured in § 5. An estimation of the sensitivity to the mixing parameters with a Dalitz-integrated analysis is performed in § 6, where phase-space efficiency and systematic errors are not taken into account. The last piece of the work is described in § 7 and consists of a first look at Run 2 data, where the impact of new triggers at HLT1 and HLT2 is studied.

3 Reconstruction of $\mathrm{D^0} \to \mathrm{K}\pi\pi^0$ decays

The analysis is based on pp collisions data collected by LHCb during 2012 and corresponding to an integrated luminosity of $2\,\mathrm{fb}^{-1}$.

The LHCb [10] detector is a single-arm forward spectrometer, designed for the study of particles containing b or c quarks. The trigger [11] consists of a hardware stage (L0), based on information from the calorimeter and muon systems followed by a two-stage software trigger (HLT). The software trigger selections used for these analysis require the presence of a displaced high-pT track at HLT1 and of a $D^{\star+} \to D^0(\to h^+h^-X)\pi^+$ decay at HLT2, where h indicates a charged hadron and X the part of the final state that is not reconstructed. The latter trigger has been implemented only in 2012, that is the reason why 2011 data are not available for this studies.

Offline, candidate $D^0 \to K^\pm\pi^\mp\pi^0$ decays are reconstructed by first selecting two charged tracks, consistent with being a kaon and a pion, forming a vertex that is well displaced from the primary pp interaction vertex. These are then combined with a $\pi^0 \to \gamma\gamma$ candidate to form a candidate D^0 decay. The neutral pions are distinguished in resolved and merged candidates according to whether the two photons from their decay result or not in well separated energy clusters in the electromagnetic calorimeter. Resolved neutral pions have better momentum resolution and cover different kinematical regions than merged π^0 candidates[1]. For these reasons resolved and merged candidates are treated separately in the analysis. Candidate D^0 decays, that are consistent with originating from the primary vertex, are then combined with a charged low-momentum track to form a $D^{\star+} \to D^0\pi^+$ decay. Finally, to improve mass resolution, a kinematical fit of the full decay topology [12] is performed by requiring that the $D^0\pi_S$ vertex to be consistent with the primary vertex and by constraining the reconstructed π^0 mass to its known value [1]. An additional fit, where also the reconstructed D^0 mass is required to be consistent with its known value [1], is used when looking at the Dalitz-plot distribution to ensure that the reconstructed events lie within the allowed kinematical region.

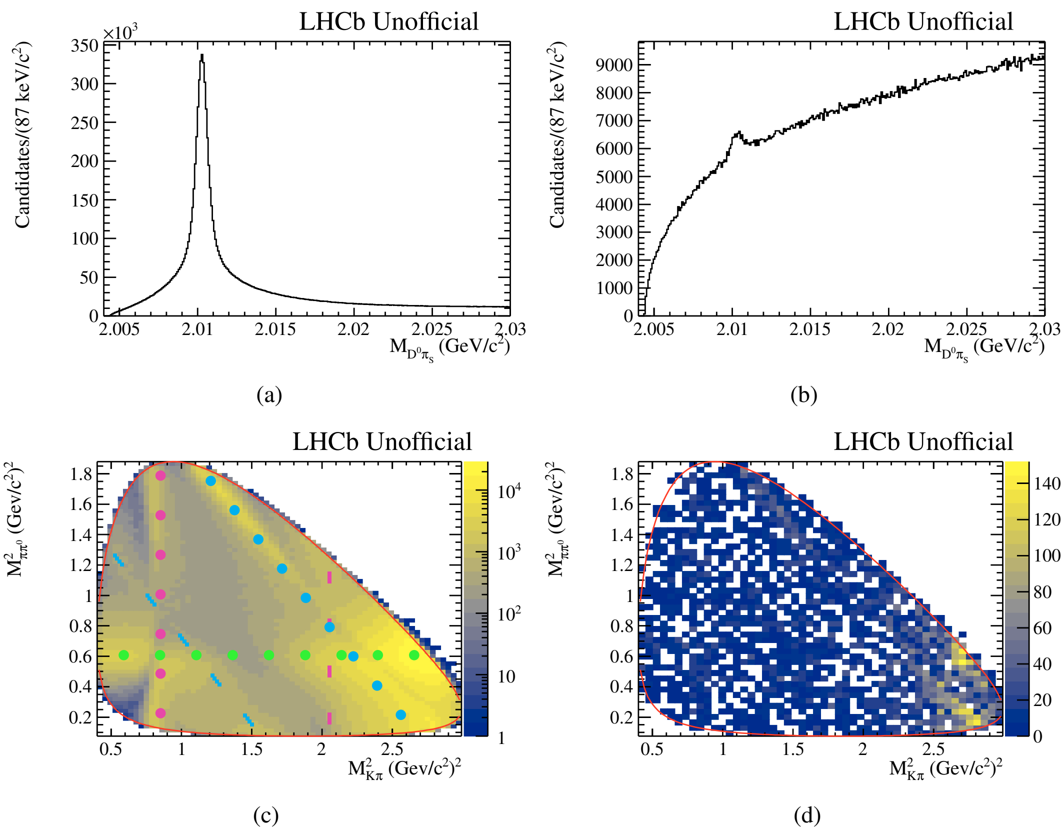

Figure 2: $M_{D^0\pi_S}$ distribution (a, b) and D^0 decay Dalitz-plot (c, d) of RS (on the left) and WS (on the right) decays for selected candidates with resolved π^0. In (c) spin-1 intermediate resonances $K^{\star 0}(892) \to K^-\pi^+$ (*red-dotted line*), $K^{\star -}(892) \to K^-\pi^0$ (*blu-dotted line*) and $\rho^+(770) \to \pi^+\pi^0$ (*green-dotted line*) as well as spin-2 resonances $K_2^0(1430) \to K^-\pi^+$ (*red-dashed line*) and $K_2^-(1430) \to K^-\pi^0$ (*blu-dashed line*) are displayed. In (d) a background subtraction from the sideband is applied. Candidates are concentrated in the high $M^2_{K\pi}$ region where the π^0 has lower momentum.

Figure 2 (3) shows the $D^0\pi_s$-mass and Dalitz-plot distributions for the selected candidates with resolved (merged) neutral pions, when the reconstructed D^0 mass is constrained to be in the range $[1825, 1910]$ MeV/c^2 ($[1800, 1950]$ MeV/c^2), corresponding to approximately two times the mass

[1]The smaller angle between the two $\gamma\gamma$ in merged π^0 reconstruction means a higher momentum for the particle.

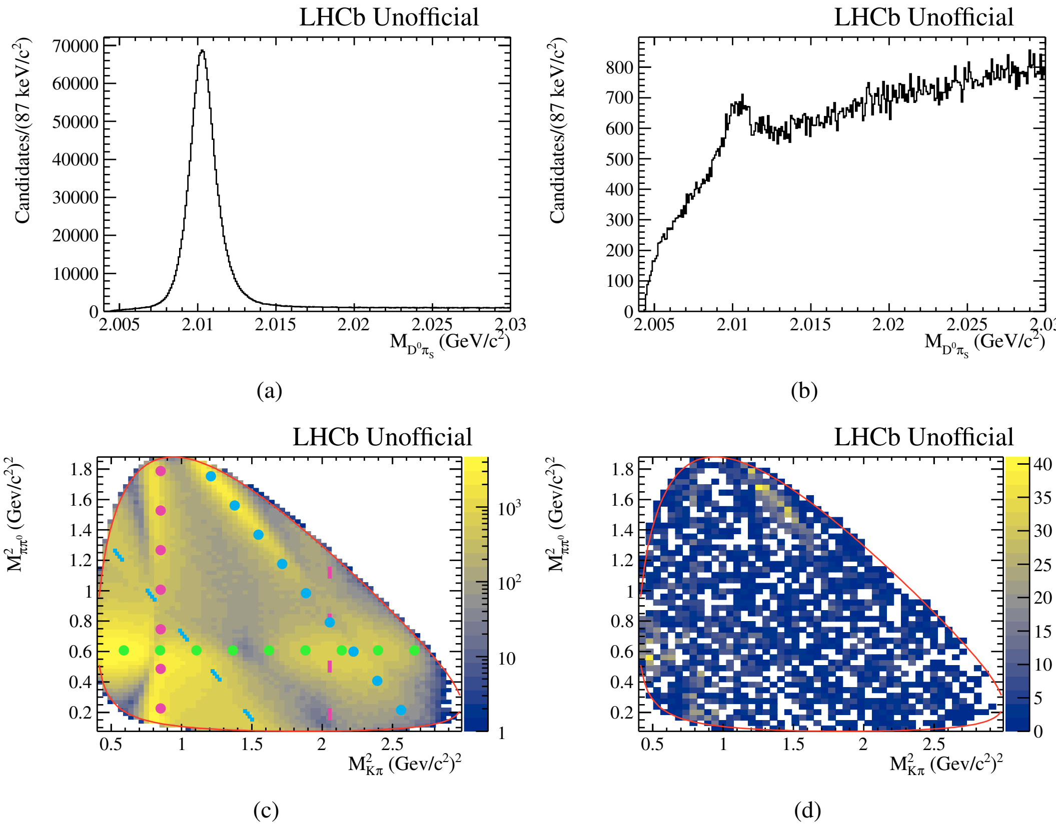

Figure 3: $M_{D^0\pi_S}$ distribution (a, b) and D^0 decay Dalitz-plot (c, d) of RS (on the left) and WS (on the right) decays for selected candidates with merged π^0. In (c) spin-1 intermediate resonances $K^{\star 0}(892) \rightarrow K^-\pi^+$ (*red-dotted line*), $K^{\star -}(892) \rightarrow K^-\pi^0$ (*blu-dotted line*) and $\rho^+(770) \rightarrow \pi^+\pi^0$ (*green-dotted line*) as well as spin-2 resonances $K_2^0(1430) \rightarrow K^-\pi^+$ (*red-dashed line*) and $K_2^-(1430) \rightarrow K^-\pi^0$ (*blu-dashed line*) are displayed. In (d) a background subtraction from the sideband is applied. Candidates are concentrated in the low $M^2_{K\pi}$ region where the π^0 has higher momentum.

resolution. In the RS sample the signal peak stands clearly over the background that is mainly composed by candidates where a correctly reconstructed D^0 is accidentally paired to a random soft pion from the primary vertex. Since WS events are rarer, the background contribution is larger. The number of RS and WS candidates obtained after this first selection is $7.0 \cdot 10^6$ ($1.7 \cdot 10^6$) and $2.2 \cdot 10^4$ ($4.9 \cdot 10^3$) for resolved (merged) π^0 sample.

From the plots one can also see that the merged π^0 candidates, despite having a worse mass resolution, show a better signal-to-background ratio. This is because, in average, D^0 candidates made with merged π^0 decays have a larger momentum than resolved ones and therefore suffer from a smaller contamination from background due to randomly-associated low momentum soft pions.

The different kinematic coverage between merged and resolved candidates can also be seen from the two complementary Dalitz-plot distributions at Fig. 2 (c)(d) and Fig. 3 (c)(d). In the resolved π^0 sample, the events are more concentrated in the right corner since π^0 has lower momentum while the merged π^0 candidates are concentrated on the left of the Dalitz-plot. This is confirmed by looking at Fig. 4, where the efficiency variation as determined on simulation is shown. Using both samples provides therefore a better coverage of the allowed phase-space.

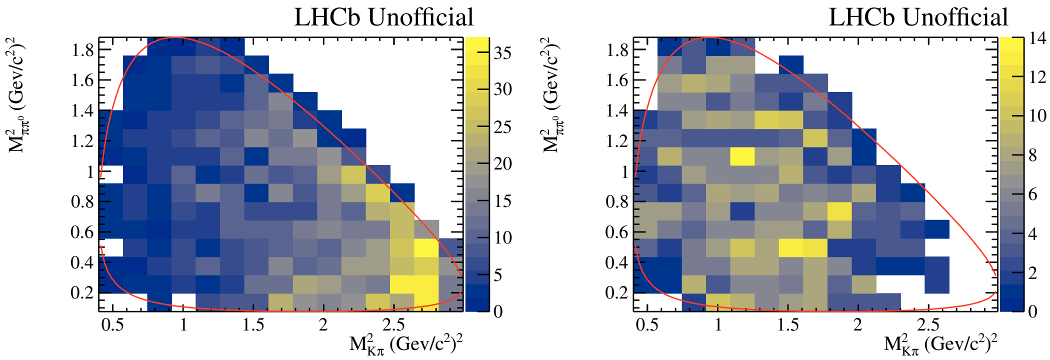

(a) (b)

Figure 4: Efficiency variation (in arbitrary units) over the Dalitz plot, as determined from simulation for resolved (a) and merged (b) π^0 RS decays.

4 Suppression of the random-pion background

To suppress the large background of random-pion candidates present in the WS sample a multivariate-analysis selection, based on the *Boosted Decision Tree* (BDT) method of the *Toolkit for Multivariate Data Analysis* [13], has been implemented.

Variable	S^2
$p_T(D^0)$	8.3%
$\cos\theta(p_T^{K\pi}, p_T^{\pi^0})$	6.5%
$CL(\pi^0)$	4.8%
$P(\pi_S \to \pi)$	3.0%
Vertex χ^2/ndf	2.5%

(a)

Variable	S^2
$p_T(\pi_S)$	7.4%
$P(\pi_S \to \pi)$	6.7%
$p(\pi_S)$	1.6%
Vertex χ^2/ndf	0.1%

(b)

Table 1: Variables used as input for the BDT training, ordered by their separation power, for resolved (a) and merged (b) π^0 sample. These are: the particle momentum p, the transverse momentum p_T and the cosine of angle θ between $p(K\pi)$ and $p(\pi^0)$ in the transverse plane; the probability for the identified X particle to be an X particle and the confidence level for the π^0 actually be a π^0; the χ^2 of the $D^\star$ vertex from the fit of the full decay topology [12], normalised to the number of degrees of freedom.

The BDT is trained with signal and background samples derived directly from data. In particular, RS candidates share the same kinematical and topological properties of the WS candidates, with the only exception of the decay time distribution. The signal and background samples are defined by requiring $|M_{D^0\pi_S} - M_{D\star}| < 0.002\,\text{GeV}/c^2$ and $2.02 < M_{D^0\pi_S} < 2.03\,\text{GeV}/c^2$ respectively. A long list of input variables have been studied trying to identify those able to better discriminate signal and background, but also with a low correlation with $M_{D^0\pi_S}$ and Dalitz-plot variables. The discrimination between signal and background is estimated computing for each variable y the statistical separation S^2, defined as

$$\langle S^2(y)\rangle = \frac{1}{2}\int \frac{(\text{pdf}_S(y) - \text{pdf}_B(y))^2}{\text{pdf}_S(y) + \text{pdf}_B(y)}dy \tag{2}$$

where $\text{pdf}_{S,B}$ are the signal and background probability density functions. The final set of variables chosen is listed in Tab. 1 and comprises variables related to the kinematic of the decay, to the identification of the particles and to the decay topology.

The resulting BDT distributions for signal and background are shown in Fig. 5 while the corresponding signal versus background separation is estimated to be 18.4% (15.1%) for the resolved (merged)

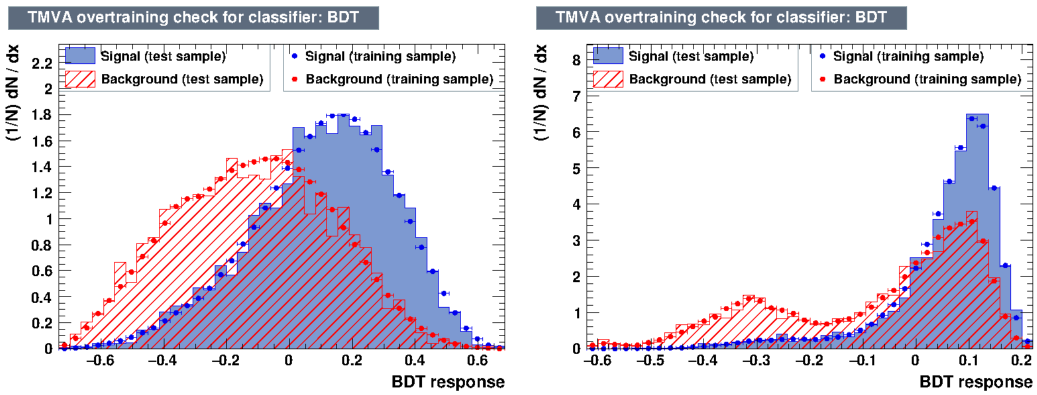

(a) (b)

Figure 5: BDT distributions for signal and backgrund as results of the training with RS decays from the full statistic (*dots*) and from an independent test sample (*line*) for resolved (a) and merged (b) π^0 candidates.

π^0 sample. Figure 5 also shows the overtraining check for the BDT: it tests that the distributions produced in BDT training are compatible with those obtained in an independent test sample.

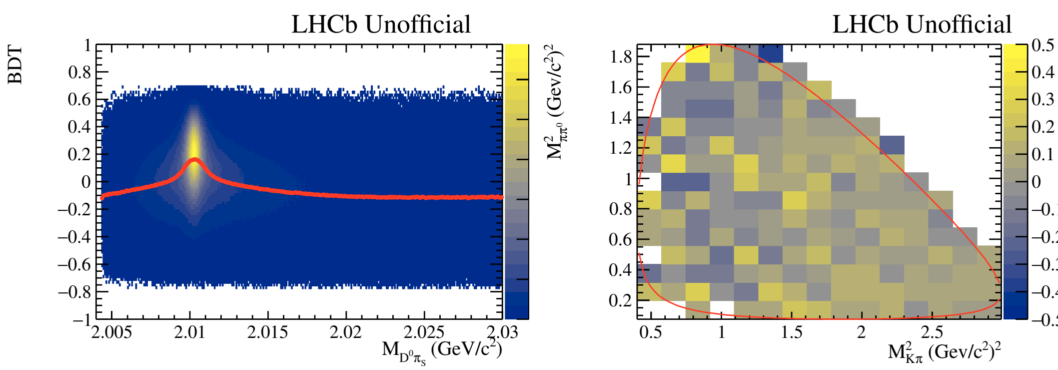

(a) (b)

Figure 6: BDT distribution and BDT average value ($\langle$BDT$\rangle$) (*red line*) as a function of $M_{D^0\pi_S}$ (a) and $\langle$BDT$\rangle$ distribution as a function of Dalitz-plot determined with simulated data (b) of RS decays for resolved π^0 sample.

To ensure no bias in the background mass shape after BDT selection, a check on the correlation of BDT with the mass $M_{D^0\pi_S}$ and Dalitz plot has been performed. As shown in Figs. 6 and 7, the correlation is small.

The optimal BDT requirement is chosen as that producing the smallest uncertainty on the measured time-integrated WS-to-RS ratio R. Therefore, many BDT requirements are tested. For each, the number of WS and RS candidates is measured by fitting the obtained $M_{D^0\pi_S}$ distributions (details on the fit are presented later), and their ratio is calculated. Figure 8 shows the uncertainty on R as a function of the BDT cut. In the resolved sample, a minimum is visible for BDT > 0.09, corresponding to about 20% improvement in precision with respect to the case where no BDT selection is applied. Only a marginal gain in resolution is observed for the merged sample, where BDT > -0.10 is chosen, suggesting that this sample is already pure enough for the purposes of our study.

An additional 20% (10%) background reduction is achieved by removing the WS candidates, whose D^0 was also used to reconstruct a good RS candidate for resolved (merged) π^0 sample. These candidates are most likely fake WS candidates where a wrong-sign π_s has been mistakenly associated to the correctly reconstructed $D^0 \to K^-\pi^+\pi^0$ candidate. Figure 9 shows the $D^0\pi_s$-mass distribution

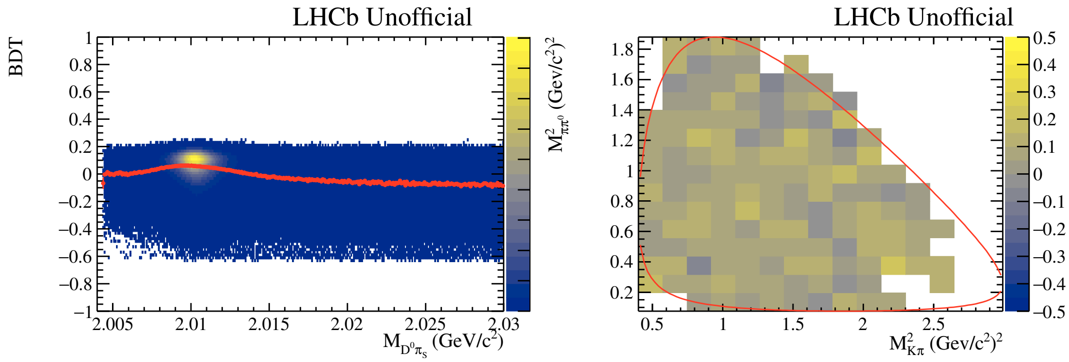

(a) (b)

Figure 7: BDT distribution and BDT average value ($\langle\mathrm{BDT}\rangle$) (*red line*) as a function of $M_{D^0\pi_S}$ (a) and $\langle\mathrm{BDT}\rangle$ distribution as a function of Dalitz-plot determined with simulated data (b) of RS decays for merged π^0 sample.

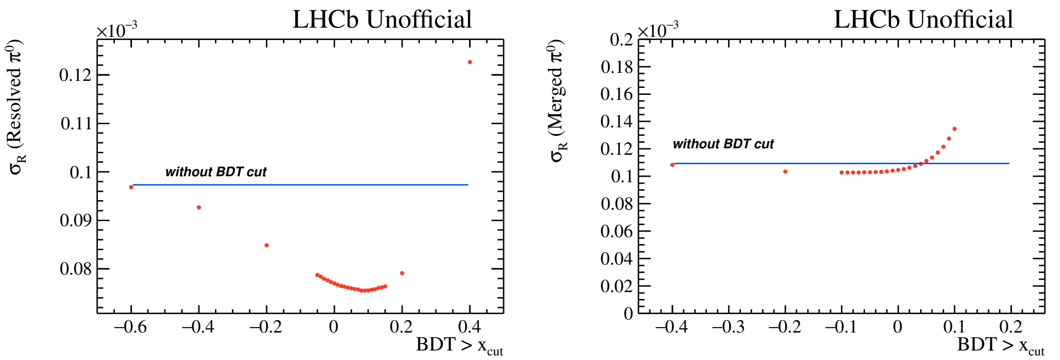

(a) (b)

Figure 8: Uncertainty on time-integrated WS-to-RS ratio as a function of the BDT cut for resolved (a) and merged (b) π^0 sample. The blue line represents this value without BDT selection.

of the removed candidates in comparison with the distribution of the candidates that are retained. The removed candidates do not show any peaking signal-like structure, as expected.

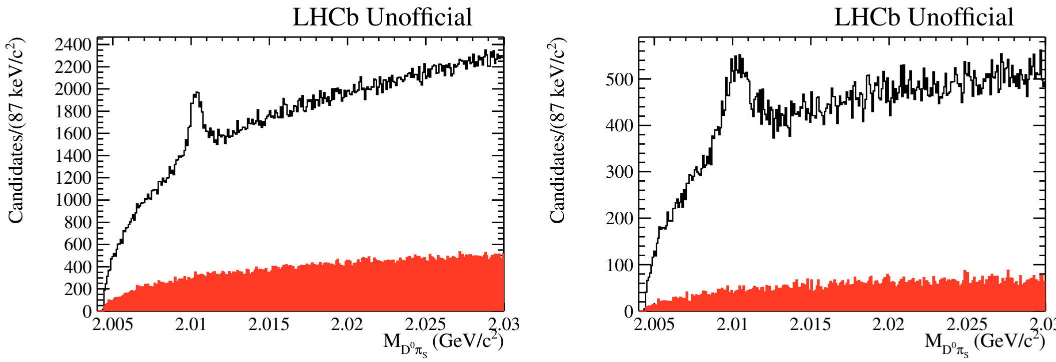

(a) (b)

Figure 9: $M_{D^0\pi_S}$ distributions after the BDT selection of WS events for resolved (a) and merged (b) π^0 sample. The distribution in red represents fake candidates where a wrong-sign π_s has been mistakenly associated to a correctly reconstructed D^0.

5 Time-integrated analysis

A binned χ^2 fit to the $M_{D^0\pi_S}$ distribution of the finally selected candidates determines the WS and RS signal yields and their ratio. In this fit the signal shape consists of a linear combination of three Gaussian functions and a Johnson SU [14] distribution:

$$\text{pdf}_S = f_0 \cdot J_{SU}(m|\mu, \delta, \lambda, \epsilon, \gamma) + f_1 \cdot G_1(m|\mu_1, \sigma_1) + f_2 \cdot G_2(m|\mu_2, \sigma_2) + f_3 \cdot G_3(m|\mu_3, \sigma_3) \quad (3)$$

The background mass shape is parameterized using the function

$$\text{pdf}_B = (m - m_0)^\alpha e^{\beta(m-m_0)}, \quad (4)$$

with m_0 fixed to the threshold value of $m_{D^0} + m_\pi = 2.004\,\text{GeV/c}^2$ [1]. All functions are properly normalized within the fit range going from the threshold up to 2.03 GeV/c^2 [2].

The fit is first performed on the RS sample with all parameters free to float. This allows to accurately determine the signal shape on the very pure and abundant RS decays. The signal shape is then fixed in the subsequent fit to the WS sample, while background parameters are kept free to float.

Figure 10 and 11 show the time-integrated $D^0\pi_s$-mass distributions with fit projections overlaid. The resulting RS and WS yields are $(3.7758 \pm 0.0065) \cdot 10^6$ $\left((1.5847 \pm 0.0035) \cdot 10^6\right)$ and $(1.024 \pm 0.027) \cdot 10^4$ $\left((4.59 \pm 0.16) \cdot 10^3\right)$ for the resolved (merged) π^0 sample, respectively. These correspond to about five times more signal candidates than what available in the full sample collected by the BaBar experiment [8].

[2]This also implies $f_3 = 1 - f_0 - f_1 - f_2$.

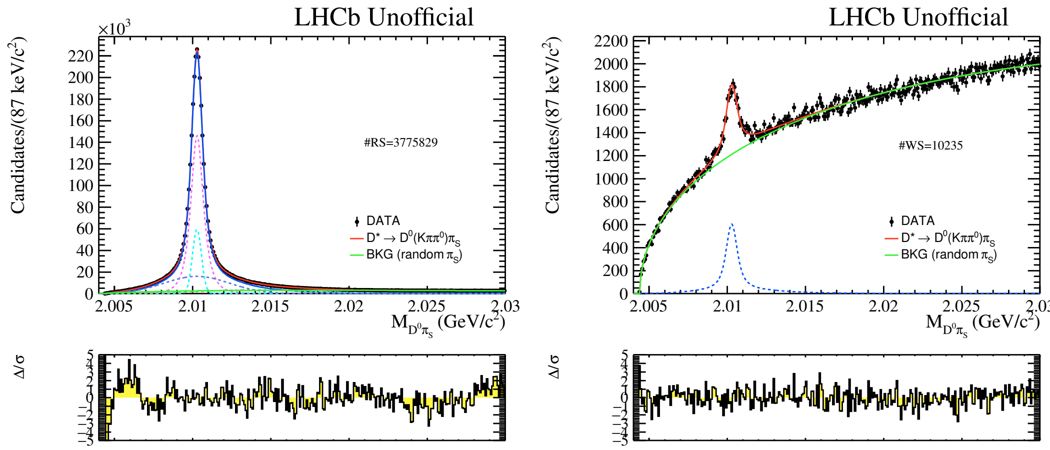

(a) (b)

Figure 10: $M_{D^0\pi_S}$ distribution of RS (a) and WS (b) candidates with resolved π^0, with fit projection overlaid and normalized residual distribution at the bottom.

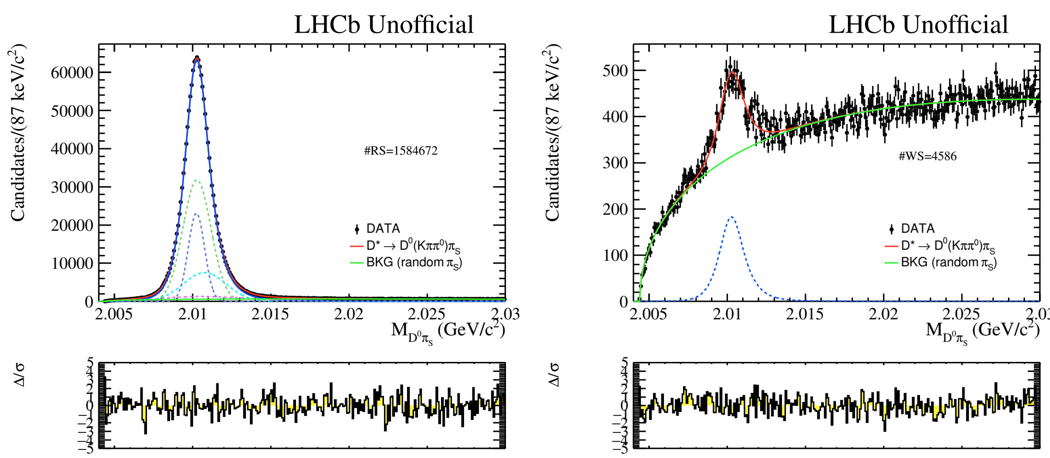

(a) (b)

Figure 11: $M_{D^0\pi_S}$ distribution of RS (a) and WS (b) candidates with merged π^0, with fit projection overlaid and normalized residual distribution at the bottom.

6 Time-dependent analysis

The samples have been divided in equally populated bins of D^0 decay time. The mass fit is repeated in each subsample with the same procedure as outlined above. Figure 12 shows the resulting WS-to-RS ratio as a function of decay time.

The distribution is fit first with a constant (no-mixing hypothesis) and then with Eq. 1 (mixing-allowed hypothesis). The results are shown in Tab. 2. By comparing the results of the two fits, the no-mixing hypothesis is excluded with a p-value of 0.08%, corresponding to approximately 3.3 Gaussian standard deviations. This is the first evidence of charm mixing in a decay channel with a neutral particle at LHCb.

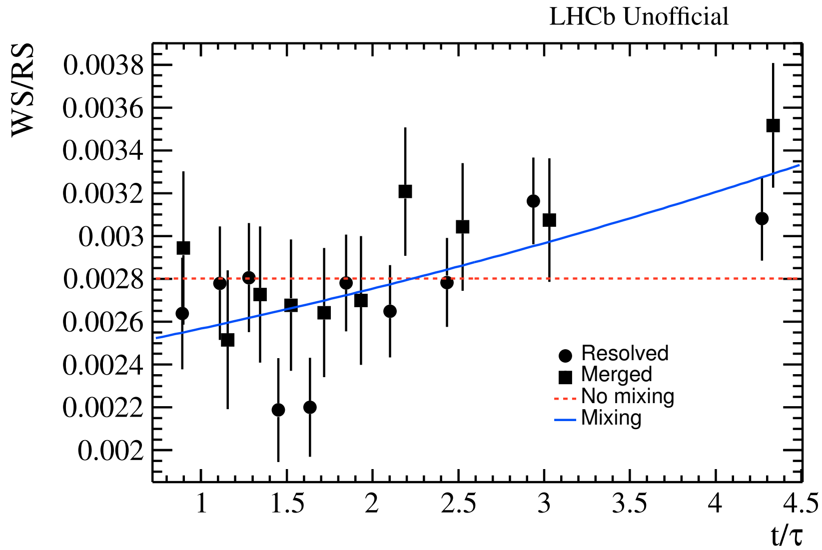

Figure 12: WS-to-RS ratio as a function of decay time.

Fit type (χ_0^2/NDF)	Parameter	Fit result
No mixing (30.3/19)	R	$(0.2802 \pm 0.0058)\%$
Mixing (16.1/17)	R_D	$(0.241 \pm 0.034)\%$
	$\alpha y'$	$(0.30 \pm 0.62)\%$
	$R_M/2$	$(0.0013 \pm 0.0055)\%$

Table 2: Results of the time-dependent fit to the data. The uncertainties don't include systematic sources and efficiency corrections on Dalitz-plot.

7 Prospects for Run 2

With the start of Run 2 the LHCb trigger has gone through substantial changes [15]. Of particular interest for the decay channel here discussed are the introduction at HLT1 of new one- and two-charged-track lines based on a multivariate discriminant, and the introduction at HLT2 of an inclusive $D^\star$ trigger based on a BDT. By the end of 2015, the inclusive $D^\star$ line has been complemented with the implementation of a set of exclusive $D^{\star+} \to D^0(\to K^\pm\pi^\mp\pi^0)\pi^+$ lines (including both resolved and merged $\pi^0 \to \gamma\gamma$ decays).

Year	N_{RS}/L (fb)	$\frac{N_{RS}/L(year)}{N_{RS}/L(2012)}$
2012	2'700'000	1
2015	6'440'000	2.4
2016	5'710'000	2.1

Table 3: Number of RS signal candidates per integrated luminosity collected during the years and the ratio of the yields compared with 2012.

Table 3 shows the number of RS signal candidates per integrated luminosity collected during the years and the ratio of the yields compared with 2012. The increase in signal yield per integrated luminosity is partially due to the larger available production cross-section at 13 TeV with respect to 7 TeV (which for charm mesons is measured to be approximately two times larger [16]) and partially to the trigger improvements. Small differences between 2015 and 2016 are expected due to different trigger thresholds and data-taking conditions.

	N_{RS}/L (fb)	
	Resolved	Merged
All candidates	$4.64 \cdot 10^6$	$1.76 \cdot 10^6$
HLT1TrackMVA	$4.56 \cdot 10^6$	$1.68 \cdot 10^6$
HLT1TwoTrackMVA	$4.02 \cdot 10^6$	$1.48 \cdot 10^6$
HLT2Inclusive	$4.12 \cdot 10^6$	$9.95 \cdot 10^5$
HLT2Exclusive	$7.03 \cdot 10^5$	$9.85 \cdot 10^5$

Table 4: Selected RS signal yields per unit luminosity in 2016 data for resolved and merged π^0 samples in terms of the different trigger lines.

Table 4 reports the breakdown of the selected RS signal yields in 2016 in terms of the different trigger lines at HLT1 and HLT2. At HLT1 most of the candidates are selected by the one-track line with approximately 2% (5%) of the resolved (merged) candidates selected only through the two-track line. At HLT2, the improvement induced by the exclusive line is more evident. In particular, about 11% (50%) of the resolved (merged) candidates are selected only by the exclusive line.

Conclusion

In summary, this work represents a first attempt to measure $D^0 - \bar{D}^0$ mixing using $D^0 \to K^\pm\pi^\mp\pi^0$ decays at LHCb. The obtained results, based on a time-dependent and Dalitz-integrated measurement of the WS-to-RS yield ratio in 2012 data, seem to be competitive with other available measurements based on these decays [7–9]. However, all results presented have to be considered preliminary and unofficial. The sensitivity to the mixing parameters could be increased with the larger statistics that is being collected during Run 2 and/or through a more sophisticated time- and Dalitz-plot-dependent analysis. For the work here presented, I have been awarded by the LHCb collaboration the Moritz Karbach prize for outstanding summer students.

References

[1] K. A. Olive et al. Review of Particle Physics. *Chin. Phys.*, C38:090001, 2014. doi: 10.1088/1674-1137/38/9/090001.

[2] Bernard Aubert et al. Evidence for $D^0 - \bar{D^0}$ Mixing. *Phys. Rev. Lett.*, 98:211802, 2007. doi: 10.1103/PhysRevLett.98.211802.

[3] M. Starič et al. Evidence for D^0-$\bar{D}^0$ mixing. *Phys. Rev. Lett.*, 98:211803, May 2007. doi: 10.1103/PhysRevLett.98.211803. URL `http://link.aps.org/doi/10.1103/PhysRevLett.98.211803`.

[4] R Aaij et al. Observation of $D^0 - \overline{D}^0$ oscillations. *Phys. Rev. Lett.*, 110(10):101802, 2013. doi: 10.1103/PhysRevLett.110.101802.

[5] Heavy Flavor Averaging Group.

[6] N. Lowrey et al. Determination of the $D^0 \to K^-\pi^+\pi^0$ and $D^0 \to K^-\pi^+\pi^+\pi^-$ Coherence Factors and Average Strong-Phase Differences Using Quantum-Correlated Measurements. *Phys. Rev.*, D80:031105, 2009. doi: 10.1103/PhysRevD.80.031105.

[7] X. C. Tian et al. Measurement of the wrong-sign decays $D^0 \to K^+\pi^-(\pi^0, \pi^+\pi^-)$ and search for CP violation. *Phys. Rev. Lett.*, 95:231801, 2005. doi: 10.1103/PhysRevLett.95.231801.

[8] Bernard Aubert et al. Search for $D^0 - \bar{D^0}$ Mixing and Branching-Ratio Measurement in the Decay $D^0 \to K^+\pi^-\pi^0$. *Phys. Rev. Lett.*, 97:221803, 2006. doi: 10.1103/PhysRevLett.97.221803.

[9] Bernard Aubert et al. Measurement of $D^0 - \bar{D}^0$ mixing from a time-dependent amplitude analysis of $D^0 \to K^+\pi^-\pi^0$ decays. *Phys. Rev. Lett.*, 103:211801, 2009. doi: 10.1103/PhysRevLett.103.211801.

[10] A. Augusto Alves, Jr. et al. The LHCb Detector at the LHC. *JINST*, 3:S08005, 2008. doi: 10.1088/1748-0221/3/08/S08005.

[11] R Aaij et al. The LHCb Trigger and its Performance in 2011. *JINST*, 8:P04022, 2013. doi: 10.1088/1748-0221/8/04/P04022.

[12] W. D. Hulsbergen. Decay chain fitting with a Kalman filter. *Nuclear Instruments and Methods in Physics Research A*, 552:566–575, November 2005. doi: 10.1016/j.nima.2005.06.078.

[13] A. Hoecker, P. Speckmayer, J. Stelzer, J. Therhaag, E. von Toerne, H. Voss, M. Backes, T. Carli, O. Cohen, A. Christov, D. Dannheim, K. Danielowski, S. Henrot-Versille, M. Jachowski, K. Kraszewski, A. Krasznahorkay, Jr., M. Kruk, Y. Mahalalel, R. Ospanov, X. Prudent, A. Robert, D. Schouten, F. Tegenfeldt, A. Voigt, K. Voss, M. Wolter, and A. Zemla. TMVA - Toolkit for Multivariate Data Analysis. *ArXiv Physics e-prints*, March 2007.

[14] Norman L Johnson. Systems of frequency curves generated by methods of translation. *Biometrika*, 36(1/2):149–176, 1949.

[15] Barbara Sciascia. LHCb Run 2 Trigger Performance. May 2016. URL `https://cds.cern.ch/record/2208038`.

[16] Roel Aaij et al. Measurements of prompt charm production cross-sections in pp collisions at $\sqrt{s} = 13$ TeV. *JHEP*, 03:159, 2016. doi: 10.1007/JHEP03(2016)159,10.1007/JHEP09(2016)013. [Erratum: JHEP09,013(2016)].